Journal of Physics: Condensed Matter

PAPER

Multiple tuning of magnetic biskyrmions using *in situ* L-TEM in centrosymmetric MnNiGa alloy

IOP Publishing Journal of Physics: Condensed Matter
J. Phys.: Condens. Matter **30** (2018) 065803 (7pp) https://doi.org/10.1088/1361-648X/aaa527

Multiple tuning of magnetic biskyrmions using *in situ* L-TEM in centrosymmetric MnNiGa alloy

Licong Peng[1,2], Ying Zhang[1], Min He[1,2], Bei Ding[1,2], Wenhong Wang[1], Jianqi Li[1,2], Jianwang Cai[1,2], Shouguo Wang[3], Guangheng Wu[1] and Baogen Shen[1,2]

[1] Beijing National Laboratory for Condensed Matter Physics, Institute of Physics, Chinese Academy of Sciences, Beijing 100190, People's Republic of China
[2] School of Physical Sciences, University of Chinese Academy of Sciences, Beijing 100049, People's Republic of China
[3] School of Materials Science and Engineering, University of Science and Technology Beijing, Beijing 100083, People's Republic of China

E-mail: zhangy@iphy.ac.cn

Received 17 November 2017, revised 25 December 2017
Accepted for publication 4 January 2018
Published 18 January 2018

Abstract

Magnetic skyrmions are topologically protected spin configurations and have recently received growingly attention in magnetic materials. The existence of biskyrmions within a broad temperature range has been identified in our newly-discovered MnNiGa material, promising for potential application in physics and technological study. Here, the biskyrmion microscopic origination from the spin configuration evolution of stripe ground state is experimentally identified. The biskyrmion manipulations based on the influences of the basic microstructures and external factors such as grain boundary confinement, sample thickness, electric current, magnetic field and temperature have been systematically studied by using real-space Lorentz transmission electron microscopy. These multiple tuning options help to understand the essential properties of MnNiGa and predict a significant step forward for the realization of skyrmion-based spintronic devices.

Keywords: magnetic biskyrmion, multiple manipulations, L-TEM, MnNiGa

(Some figures may appear in colour only in the online journal)

1. Introduction

Nanometric magnetic skyrmions with topologically nontrivial spin configurations, have attracted a rich interest in chiral magnetic materials with Dzyaloshinskii–Moriya interaction. Many fascinating physical features such as emergent electromagnetic fields [1–3] and ultralow current-driven behavior [4–6], enable the potential applications of skyrmions in memory device as prime candidates. This vortex-like skyrmion configuration, swirling to wrap a 3D spherical surface unit with spins pointing in all directions, was originally proposed by Skyrme [7] as a model for hadrons, then was predicted existing in magnetic materials by many theoretical works [8–10]. Recently, the experimental breakthroughs have been made in the study of skyrmion existence and stability, the topologically physical properties [3, 4, 11], and the manipulation behaviors under external stimulus such as temperature [12], magnetic field [11, 13] and electric current [4, 6] in chiral helimagnets. However, the narrow magnetic field (B) and temperature (T) range for equilibrium skyrmions in most chiral materials (below room temperature), limits the application, thereby proposing desperate need for discovery of various skyrmion material systems within broad temperature range including room temperature.

Magnetic skyrmions in dipolar magnets have been studied experimentally in centrosymmetric bulk systems [14–16] and theoretically described in Hamiltonian model [17] as a consequence of mutual competition between different energy terms such as dipolar, anisotropy and exchange interactions. Unlike the fixed spin helicity of chiral-type skyrmions introduced by the crystallographic broken inversion symmetry, skyrmions in centrosymmetric magnets allow two helicity degrees of freedom selected at random [1, 18]. To identify different spin configurations, the topological number is defined to count how many times the spins wrapping the unit sphere [11, 14]. For skyrmions in chiral magnets, the topological number is 1 with only one unique helicity. Recently a new biskyrmion configuration with two oppositely swirling spins possessing topological number 2, is discovered and fully explained in dipolar magnets such as tetragonal manganite $La_{2-2x}Sr_{1+2x}Mn_2O_7$ ($x = 0.315$) below 60 K [14], Fe/Gd thin film at 300 K [19] and our hexagonal $(Mn_{1-x}Ni_x)_{65}Ga_{35}$ ($x = 0.5$) (MnNiGa) alloy over 16 K–338 K [16, 20]. Regardless of the various spin configurations, the non-zero topological number is the key factor to drive skyrmions by electric currents, which can be presented as nontrivial skyrmions by topological Hall resistivity [3, 16].

The existence of biskyrmion configuration and the realization of zero-field biskyrmion lattice in super-wide operating temperature via manipulations in our MnNiGa material [16, 20, 21], drive us to fully investigate the microscopic origins, prompting the application in skyrmion-based spintronic devices. In this work, the magnetic microstructures of the stripe domains and biskyrmions have been interpreted by using real-space Lorentz transmission electron microscopy (L-TEM). Multiple influential factors such as confined geometry, electric current, magnetic field, thickness and temperature, have been extensively analyzed to help in understanding the essential properties of skyrmion generation in MnNiGa. This easily fabricated MnNiGa material hosting skyrmions with multiple tuning options in wide temperature range indicates significant progress toward the realization of skyrmion-based spintronic information storage.

2. Materials and methods

$(Mn_{1-x}Ni_x)_{65}Ga_{35}$ ($x = 0.5$) (MnNiGa) polycrystalline is fabricated by arc melting method as elaborated in [16]. The hexagonal structured MnNiGa crystal exhibits uniaxial (c-axial) anisotropy due to Mn canting [16, 22] and thus the individual grain is observed along [0 0 1] zone axis to better reflect the morphology of biskyrmion in our TEM study. The magnetic skyrmion evolution at different temperatures is imaged by L-TEM (JEOL 2100F and Tecnai F20) equipped with double-tilt liquid-nitrogen holder and liquid helium holder. *In situ* current-driven biskyrmion motion is carried out by using an electrical TEM holder with the dc current supplied by a current source (Keithley 2601B). The perpendicular magnetic field is applied by exciting the magnetic objective lens of the TEM. The phase distribution based on the chemical composition is analyzed by high-angle annular dark-field (HAADF) scanning transmission electron microscopy (STEM) imaging technique on Tecnai F20 TEM. With the use of the Fresnel L-TEM method, the magnetic domain walls can be imaged as bright contrast (converging beam) or dark contrast (diverging beam) on the defocused image planes by applying a nominal defocus value of about 500 μm. The high-resolution lateral magnetization maps are reconstructed by using a phase-retrieval QPt software based on the transport of intensity equation [23].

3. Results and discussions

3.1. Magnetic microstructure analysis of the stripe domain

From the microscopic point of view, the spin configuration evolution from stripe ground state to biskyrmions is illustrated in centrosymmetric MnNiGa based on the L-TEM results in figure 1. The delicate magnetic microstructures along $[\bar{1}\,0\,1]$ and [0 0 1] directions (identified by the diffraction patterns in figures 1(e) and (j)) are demonstrated respectively in the two columns. The difference of the domain wall contrast in figures 1(a) and (f) is further manifested by their corresponding magnetization maps (figures 1(b) and (g)), phase maps (figures 1(c) and (h)) and the M_y magnetization profiles (figures 1(d) and (i)). More information about the magnetic microstructure features of the stripe domain are observed along [0 0 1] direction, which better reflects the intrinsic domain structure since it is along the easy-axis magnetization direction. When deviated from [0 0 1] direction, these fine domain structures are hidden under the mixed in-plane magnetization projection including the tilted perpendicular magnetic component. Based on the fine domain features, the spin configuration of stripe ground state is derivate to be a periodic canting spin structure as schematically shown in figure 1(k), which is energetically determined by the competition between magnetic dipolar, anisotropy and exchange interactions in centrosymmetric structure [17]. With gradually magnetizing towards the external magnetic fields, this periodic stripe domains are broken and transformed into biskyrmion configurations with topological number 2, which is energetically stable [24] and consistent with the previous biskyrmions study [14, 16, 19]. With further increasing the field, the biskyrmion state is completely turned into saturated state. Therefore, the microscopic origins of biskyrmions are attributed to the spontaneously periodic canting configuration of stripe domain.

3.2. Grain boundary confinement effects on the generation of biskyrmions

The confinement effects on biskyrmions were respectively revealed in the annealed and non-annealed samples with different grain sizes. Figure 2(a) shows the randomly scattered distribution of biskyrmions in the annealed sample, where the grain size is larger than 5 μm. The biskyrmion density is significantly increased in the non-annealed sample with smaller grains about 1 μm (figure 2(b)) and biskyrmions preferentially form close to the grain boundary as marked with yellow circles. The grain boundaries are identified as Ga-rich non-magnetic components by the HAADF-STEM image (figure

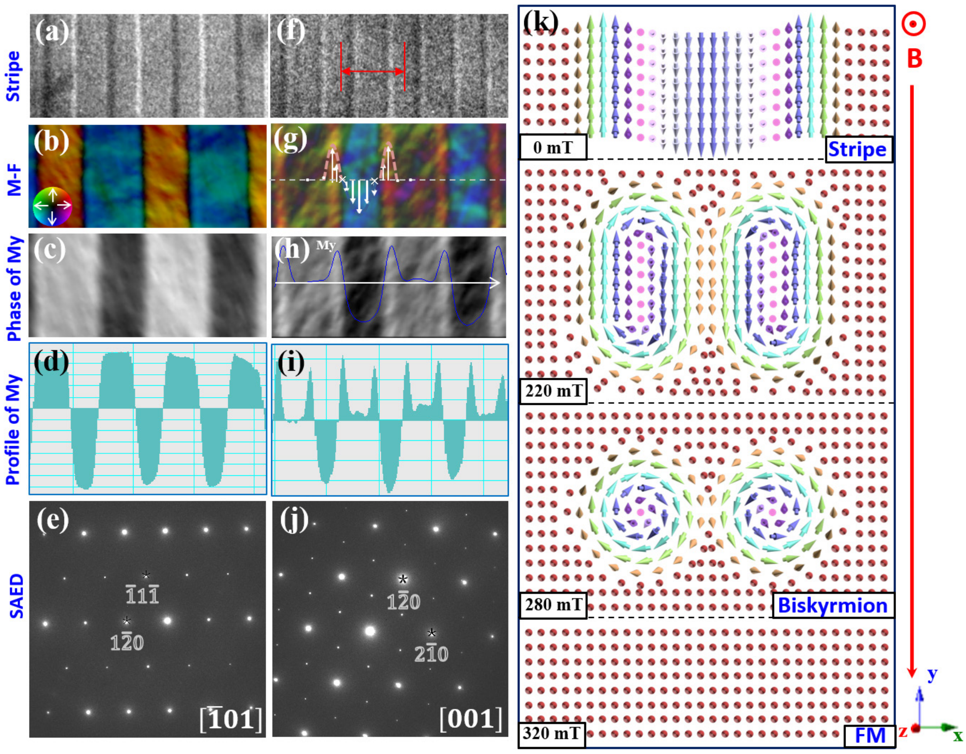

Figure 1. Magnetic microstructure analysis of the stripe ground state along two directions. (a) and (f) Under-focused L-TEM images; (b) and (g) corresponding magnetization maps; (c) and (h) phase maps of M_y; (d) and (i) the magnetization profiles of M_y; (e) and (j) diffraction patterns taken along $[\bar{1}\,0\,1]$ and [0 0 1] zone axis respectively. (k) Schematic illustration of the biskyrmion evolution from stripe domains as a function of magnetic field.

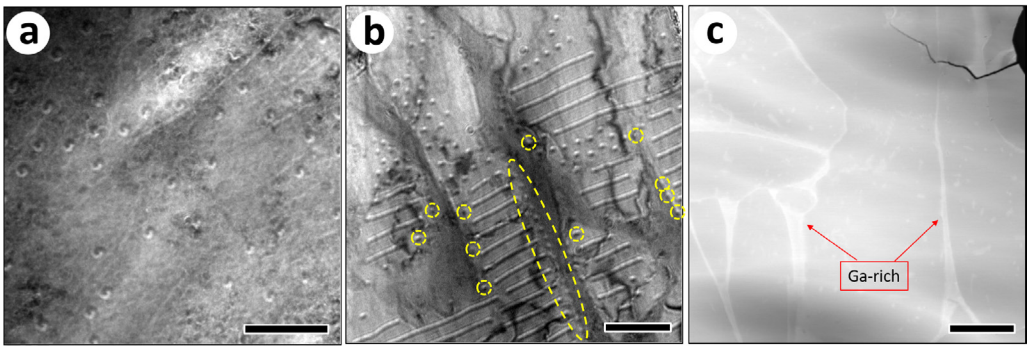

Figure 2. L-TEM images of annealed (a) and non-annealed (b) MnNiGa sample, showing the grain boundary confinement effects on the biskyrmion generation. The yellow circles in (b) showing the prior biskyrmion generation at the vicinity of the grain boundary. (c) HAADF-STEM image showing the Ga-rich grain boundary for the non-annealed sample. The scale bar is 1 μm.

2(c)) where the intensity is proportional to the mean square of atomic number (Z^2). Near the grain boundary, the spins of stripe domain tend to tilt into the plane and orient parallel to the boundary due to the edge confinement, thus inducing an unbalanced spin torque originating from the axial magnetic anisotropy [25–28]. The prior biskyrmion generation in the vicinity of the boundary should be primarily induced by the edge instability of the stripe domain [28] and the pinning effects from defects. And the perpendicular magnetic field required to evolve stripes into the complete biskyrmion state is lower in the confined grains (0.28 T) compared with the annealed one (0.40 T). The reduced magnetic field due to edge confinement and previous studies about artificially patterned structures [29–32] indicate that zero-field biskyrmions might be realized via appropriate confined geometry in MnNiGa, which would allow for more freedoms to precisely control skyrmion behaviors.

3.3. Electric current effects on biskyrmion generation and creep motion

Our previous study [21] has demonstrated that the biskyrmion density can be greatly increased due to the electromagnetic manipulation if the electric current is pre-applied before the biskyrmion phase transition. Here, the coexistence of biskyrmions and stripes under the fixed magnetic field of 0.22 T signifies the ongoing magnetic domain transition, and then the electric current is increased to investigate the induced dynamic

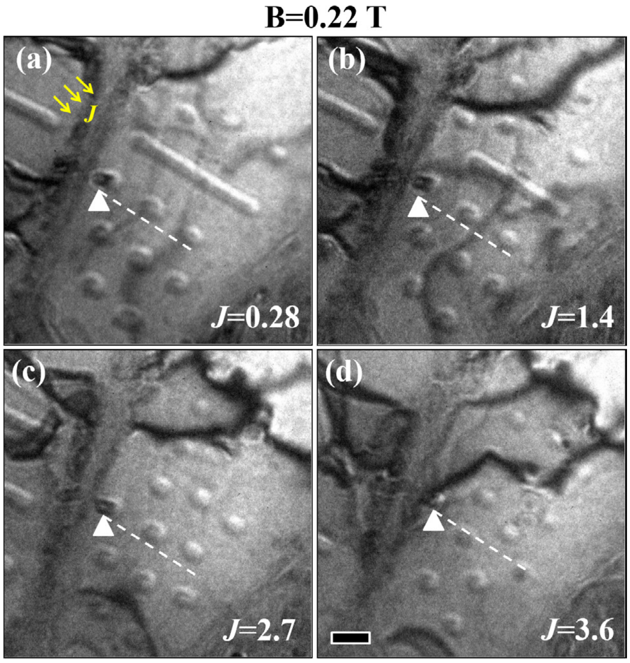

Figure 3. Biskyrmion generation and creep motion with the current density of (a) 0.28×10^7 A m^{-2}, (b) 1.4×10^7 A m^{-2}, (c) 2.7×10^7 A m^{-2}, (d) 3.6×10^7 A m^{-2} under a fixed magnetic field of 0.22 T at the vicinity of magnetic domain transition. Marks with white triangle and line for comparison. The yellow arrows represent the current direction. The scale bar in (d) is 200 nm.

biskyrmion behavior. The current density of 0.28×10^7 A m^{-2} barely has influence on the mixed state as shown in figure 3(a). With further increasing the current density up to 1.4×10^7 A m^{-2} (figure 3(b)) and 2.7×10^7 A m^{-2} (figure 3(c)) respectively, the stripes shrink and then break into biskyrmions. This skyrmion generation is mainly introduced by spin transfer torque [27] and the magnetization instability during the magnetic domain transition since the Joule heating effect is minor [21].

When the excitation of current density is further increased above 3.6×10^7 A m^{-2}, the biskyrmion creep motion is observed, presenting as the relatively changed positions as shown in figure 3(d). This striking creep motion should primarily attribute to the spin transfer torque effects between the interaction of the non-coplanar Bloch-type biskyrmion and the conduction electrons, where the biskyrmions obtain a drift velocity via the spin-motive force under the excitation of current [4, 27, 28]. In addition, the biskyrmion translation motion is limited inside the grain and cannot surmount the grain boundary obstacle due to the high energy barrier and the defect pinning effects. Generally, this current-induced biskyrmion behavior is different from the dynamic behavior of traditional trivial bubbles, where the bubble domains either collapse without moving or growing in the current direction [33].

3.4. Higher current pre-treatment effects on the residual domains

Enlightened by our previous field-cooling thermal manipulation [20], here high electric current is used as an alternative heating provider [34] for convenient technology application. Joule heating effects should be taken into account when the electric current is higher than a critical value [21]. The temperature for the high current density of 8.4×10^7 A m^{-2} is slightly higher than 350 K, which can be inferred from the gradual disappearance of magnetic domains above Curie temperature ($T_C \sim 350$ K). The relationship between the distributions of biskyrmions and manipulation procedures under different fields is summarized in figure 4. Under a small fixed magnetic field, the electric current is increased over 8.4×10^7 A m^{-2} to extinguish the stripe domains and then switched off, introducing different residual magnetic domains via varying the fixed magnetic field as shown in figures 4(a)–(d) (marked out by number 1 state). The highest biskyrmion density (figure 4(c)) is only generated after the manipulation at an optimized fixed magnetic field of about 50 mT in comparison to the mixed state of stripes and biskyrmions at both low magnetic fields (figures 4(a) and (b)) and at high magnetic field (figure 4(d)). The experimental procedure (similar to field cooling) is schematically illustrated in the inset of figure 4(a) with the corresponding L-TEM images acquired at the numbered conditions. This procedure to obtain the residual state is different from that used in [21], where the magnetic field is increased up to the saturated ferromagnetic state and then switched off under a small fixed current. These residual magnetic domain states (state number 1) evolve into complete skyrmion state with varied densities when further increasing the magnetic fields as shown in figures 4(e) and (h) (state number 2). The tunable biskyrmion density via convenient electric current manipulation facilitates the technological implements in spintronic devices.

3.5. Sample tilting effects on the magnetic skyrmion morphology

To explore the magnetic biskyrmion morphology, the residual biskyrmions at zero field are tilted to different angles in L-TEM. Different from the Néel-type skyrmions in multilayer films, where the significant contrast of magnetic domain wall only appears when tilting away from the perpendicular anisotropy direction [35, 36], the domain contrast in the Bloch-type biskyrmions always exists at any tilting angle although the spin configuration is severely distorted due to the lateral magnetic projection effects as shown in figure 5.

The biskyrmion configuration in figures 5(a)–(c) is along the [0 0 1] easy axis of the sample, evidenced by the diffraction pattern. When tilting the sample slightly away from the easy axis, the biskyrmion size appears to be larger (figures 5(d)–(f)) due to the increased in-plane magnetization component projected from the 3D biskyrmions. While further tilting with a remarkable angle, the biskyrmion distortion becomes more severe with larger size (figures 5(g)–(i)) and connected to each other (figures 5(j)–(l)). Despite this distortion, the spin configurations and topological number at different tiling angles seem to be consistent with two opposite spin helicities. Unlike the traditional magnetic bubbles with random types of spin helicities in centrosymmetric ferromagnets [18, 37, 38], the

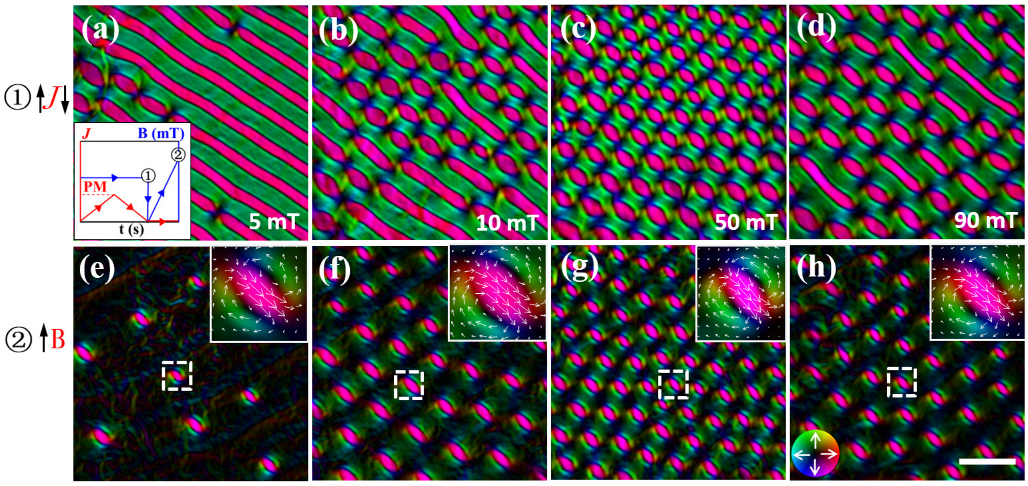

Figure 4. The residual domains obtained after high current pre-treatments at different magnetic fields of (a) 5 mT, (b) 10 mT, (c) 50 mT and (d) 90 mT. (e)–(h) Further increasing the magnetic field from residual state to complete skyrmion state. The inset of (a) presenting a schematic manipulation procedure plot to better demonstrate how the electric current and magnetic field are applied. PM for paramagnetic state. The scale bar in (h) is 500 nm.

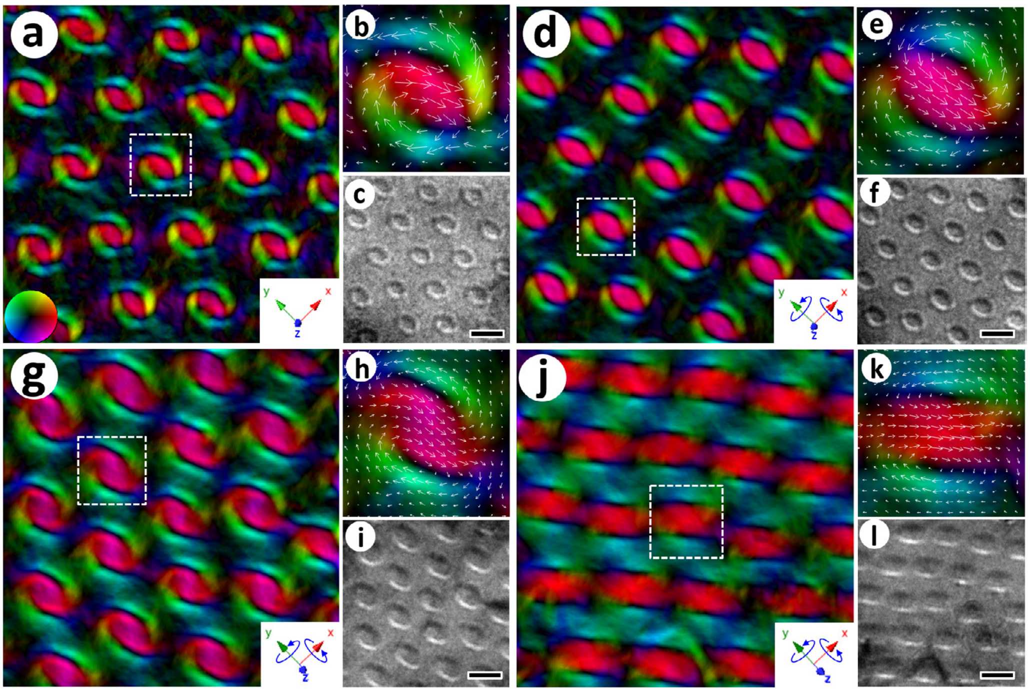

Figure 5. Magnetic biskyrmion morphology dependence of sample tilting. (a) The in-plane magnetization projection of skyrmions near [0 0 1] direction. (b) The enlarged depicted biskyrmion. (c) The under-focused L-TEM image. Biskyrmion configurations at a tilting angle of (d)–(f) Δx 7.8°, Δy 0.3°, (g)–(i) Δx 15.9°, Δy 9.8°, and (j)–(l) Δx 18.7°, Δy 19.7° away from the [0 0 1] zone axis. The scale bar is 200 nm.

topological number for biskyrmion is always 2 with uniform spin configuration.

3.6. In-plane magnetic field effects on biskyrmion spin configuration

The orientation of stripe domain and the biskyrmion spin configuration can be manipulated by the in-plane magnetic field as shown in figure 6. The manipulation procedure includes first increasing the external perpendicular magnetic field to saturate the stripe domains into uniform ferromagnetic state, and then tilting the sample to a certain angle, thereby introducing projected in-plane magnetic field. Here, in-plane magnetic fields work in two different ways. While going through the transition from saturated state to stripes via lowering magnetic fields, in-plane magnetic fields assist the generation of preferred stripe orientation as shown in figures 6(a), (c) and (e). Then the skyrmion deformation (figures 6(b), (d) and (f)) due to in-plane magnetic fields is similar to the previous theoretical and experimental work [39, 40]. The in-plane magnetic fields enlarge the region with parallel magnetization while shrink the opposite one, thereby changing the

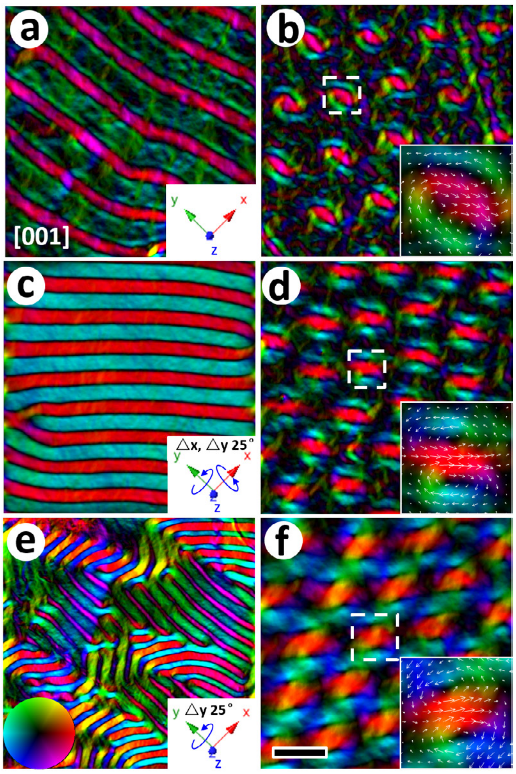

Figure 6. Biskyrmion spin configuration dependence on in-plane magnetic fields. (a) Initial stripe domain and (b) corresponding biskyrmion state near [0 0 1] zone axis. (c) and (d) L-TEM images of orientated stripes at the tilting angle of Δx 25° and Δy 25°, and (e) and (f) Δy 25° away from [0 0 1]. The insets of (a), (c) and (e) show the coordinates for tilting reference. The insets of (b), (d) and (f) show the in-plane magnetization distributions of the enlarged biskyrmion. The scale bar is 200 nm.

magnetization components of the biskyrmion configuration accordingly. The tunable orientations of the stripe domains are observed at an angle about 60°. The irregular stripes emerge at a certain angle (figure 6(e)) due to the energy competition but the skyrmion number is unchanged (figure 6(f)) thanks to the topological protection. Therefore, the biskyrmion spin configuration arrangement can be controlled by the in-plane magnetic fields, which gives additional manipulation option for skyrmion configuration.

3.7. Sample thickness influences on biskyrmion dynamics

The dynamic biskyrmion generation could be influenced by sample thickness as demonstrated in figure 7. The wedge-shaped thickness gradient (the inset of figure 7(d)) is induced from the TEM sample preparation, with the increased thickness from the edge along the dark arrow. The biskyrmion annihilation process based on the zero-field residual biskyrmion lattice after FC manipulation [20], is demonstrated in figures 7(a)–(d) with the temperature increasing from 300 K to 326 K under a constant magnetic field of 0.15 T. The biskyrmion size is strongly dependent on the temperature and the sample thickness. When the temperature is above 315 K (figure 7(b)), the biskyrmion sizes start to shrink from thinner region with larger size at the thicker region. The biskyrmion contrast

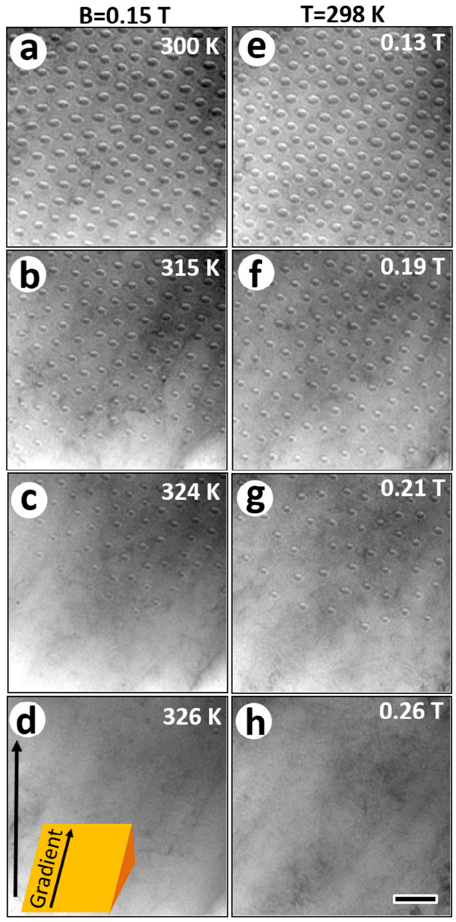

Figure 7. Biskyrmion distribution dependence on sample thickness. (a)–(d) Biskyrmion annihilation process as a function of temperature at 0.15 T. (e)–(h) Biskyrmion annihilation process as a function of magnetic field at room temperature. The inset of (d) shows the schematic sample thickness gradient. The L-TEM images of (a) and (e) are based on the zero-field residual biskyrmions after field cooling manipulation similar to our previous work [20]. The scale bar is 500 nm.

diminishes first at the thinner region above 324 K (figure 7(c)) and then followed by the thicker area (figure 7(d)), which is much lower than the Curie temperature (350 K) due to the assistance of 0.15 T magnetic field. A similar biskyrmion annihilation process via increasing the magnetic field from 0.13 T to 0.26 T at the same region, is studied at room temperature as shown in figures 7(e)–(h). The complete biskyrmion state with different sizes is observed at 0.13 T (figure 7(e)) and the size starts to shrink at 0.19 T (figure 7(f)). The biskyrmions in thinner region vanish above 0.21 T (figure 7(g)) lower than the annihilation field of 0.26 T at relatively thick region (figure 7(h)). For the dipolar magnets like MnNiGa, the competition between uniaxial anisotropy and the dipolar interaction is dominant for the skyrmion generation. Higher magnetic fields are required in thicker samples to generate skyrmions from stripe domains and to annihilate skyrmions into the saturated state. Thus, the biskyrmions in the thinner region are easier to be affected by external fields, preferentially appearing or disappearing while changing the magnetic field or temperature and the biskyrmions in the thick region are more robust against external disturbances.

4. Summary

In conclusion, multiple possibilities to manipulate biskyrmions are studied in the hexagonal MnNiGa magnet by systematically real-space L-TEM observations. The grain boundary restriction and defects are beneficial to the generation and stability of biskyrmions but not good for continuous driving motion. Only creep motion is observed at lower electric current. The significant Joule heating effects at higher electric current density provide alternative method to generate high-density biskyrmion lattice similar to field cooling manipulation. The arrangement of biskyrmion configuration can be manipulated via tilting the sample based on the in-plane magnetic fields. Additionally, the sample thickness could affect the skyrmion stability against external disturbances. Our finding extends the possible alternatives for manipulating the topological biskyrmion configuration in our newly discovered MnNiGa material, prompting applications in information storage devices.

Acknowledgments

This work was supported by National Natural Science Foundation of China (Grants 11374349, 51590880, 51431009, 51561145003, 51625101), Youth Innovation Promotion Association, CAS, 2015004.

ORCID iDs

Licong Peng https://orcid.org/0000-0002-8580-2285
Ying Zhang https://orcid.org/0000-0001-5476-1524
Wenhong Wang https://orcid.org/0000-0002-0641-3792

References

[1] Nagaosa N, Yu X Z and Tokura Y 2012 *Phil. Trans. R. Soc.* A **370** 5806–19
[2] Fert A, Cros V and Sampaio J 2013 *Nat. Nanotechnol.* **8** 152–6
[3] Neubauer A, Pfleiderer C, Binz B, Rosch A, Ritz R, Niklowitz P G and Boni P 2009 *Phys. Rev. Lett.* **102** 186602
[4] Liang D, Degrave J P, Stolt M J, Tokura Y and Jin S 2015 *Nat. Commun.* **6** 8217
[5] Jonietz F *et al* 2010 *Science* **330** 1648–51
[6] Yu X Z, Kanazawa N, Zhang W Z, Nagai T, Hara T, Kimoto K, Matsui Y, Onose Y and Tokura Y 2012 *Nat. Commun.* **3** 988
[7] Skyrme T H R 1962 *Nucl. Phys.* **31** 556–69
[8] Rößler U K, Bogdanov A N and Pfleiderer C 2006 *Nature* **442** 797–801
[9] Bak P and Hsgh Jensen M 1980 *J. Phys. C Solid State Phys.* **13** 881–5
[10] Binz B and Vishwanath A 2006 *Phys. Rev.* B **74** 214408
[11] Nagaosa N and Tokura Y 2013 *Nat. Nanotechnol.* **8** 899–911
[12] Yu X, Kikkawa A, Morikawa D, Shibata K, Tokunaga Y, Taguchi Y and Tokura Y 2015 *Phys. Rev.* B **91** 54411
[13] Yu X Z, Onose Y, Kanazawa N, Park J H, Han J H, Matsui Y, Nagaosa N and Tokura Y 2010 *Nature* **465** 901–4
[14] Yu X Z, Tokunaga Y, Kaneko Y, Zhang W Z, Kimoto K, Matsui Y, Taguchi Y and Tokura Y 2014 *Nat. Commun.* **5** 3198
[15] Yu X Z, Shibata K, Koshibae W, Tokunaga Y, Kaneko Y, Nagai T, Kimoto K, Taguchi Y, Nagaosa N and Tokura Y 2016 *Phys. Rev.* B **93** 134417
[16] Wang W *et al* 2016 *Adv. Mater.* **28** 6887–93
[17] Koshibae W and Nagaosa N 2016 *Nat. Commun.* **7** 10542
[18] Yu X, Mostovoy M, Tokunaga Y, Zhang W, Kimoto K, Matsui Y, Kaneko Y, Nagaosa N and Tokura Y 2012 *Proc. Natl Acad. Sci.* **109** 8856–60
[19] Lee J C T *et al* 2016 *Appl. Phys. Lett.* **109** 22402
[20] Peng L *et al* 2017 *Nano Lett.* **17** 7075–9
[21] Peng L *et al* 2017 *npj Quantum Mater.* **2** 30
[22] Shiraishi H, Niida H, Iguchi Y, Mitsudo S, Motokawa M, Ohayama K, Miki H, Onodera H, Hori T and Kanematsu K 1999 *J. Magn. Magn. Mater.* **196–7** 660–2
[23] Ishizuka K and Allman B 2005 *J. Electron Microsc.* **54** 191–7
[24] Lilliehöök D, Lejnell K, Karlhede A and Sondhi S L 1997 *Phys. Rev.* B **56** 6805–9
[25] Lee S H, Zhu F Q, Chien C L and Markovic N 2008 *Phys. Rev.* B **77** 132408
[26] Du H *et al* 2015 *Nat. Commun.* **6** 8504
[27] Lin S Z 2016 *Phys. Rev.* B **94** 020402
[28] Yamaguchi A, Ono T, Nasu S, Miyake K, Mibu K and Shinjo T 2004 *Phys. Rev. Lett.* **92** 77205
[29] Sun L, Cao R X, Miao B F, Feng Z, You B, Wu D, Zhang W, Hu A and Ding H F 2013 *Phys. Rev. Lett.* **110** 167201
[30] Miao B F *et al* 2014 *Phys. Rev.* B **90** 174411
[31] Zheng F *et al* 2017 *Phys. Rev. Lett.* **119** 197205
[32] Beg M *et al* 2015 *Sci. Rep.* **5** 17137
[33] Tanaka M, Kanazawa H, Sumitomo S, Honda S, Mibu K and Awano H 2015 *Appl. Phys. Express* **8** 73002
[34] Oike H, Kikkawa A, Kanazawa N, Taguchi Y, Kawasaki M, Tokura Y and Kagawa F 2016 *Nat. Phys.* **12** 62–6
[35] Jiang W *et al* 2015 *Science* **349** 283–6
[36] Benitez M J, Hrabec A, Mihai A P, Moore T A, Burnell G, McGrouther D, Marrows C H and McVitie S 2015 *Nat. Commun.* **6** 8957
[37] Grundy P J and Herd S R 1973 *Phys. Status Solidi* **20** 295–307
[38] Morikawa D, Yu X Z, Kaneko Y, Tokunaga Y, Nagai T, Kimoto K, Arima T and Tokura Y 2015 *Appl. Phys. Lett.* **107** 212401
[39] Wang C, Du H, Zhao X, Jin C, Tian M, Zhang Y and Che R 2017 *Nano Lett.* **17** 2921–7
[40] Lin S-Z and Saxena A 2015 *Phys. Rev.* B **92** 180401